Textile & Leather Review

ISSN 2623-6281 | www.tlr-journal.com | 10.31881/TLR

Circadian-Oriented Multi-Channel LED Spectral Optimization Using Differential Evolution and Constrained Nonlinear Programming

Jinwang Luo

How to cite: Luo J. Circadian-Oriented Multi-Channel LED Spectral Optimization Using Differential Evolution and Constrained Nonlinear Programming. Textile & Leather Review. 2026; 9:2941-2977. https://doi.org/10.31881/TLR.2026.2941

How to link https://doi.org/10.31881/TLR.2026.2941

Published:25 April 2026

Circadian-Oriented Multi-Channel LED Spectral Optimization Using Differential Evolution and Constrained Nonlinear Programming

Jinwang Luo

College of Information and Intelligence, Hunan Agricultural University, Changsha 410128, Hunan, China
luoyeyiyouguitu@gmail.com

Article
https://doi.org/10.31881/TLR.2026.2941
Published 25 April 2026

ABSTRACT

Light is a visual medium and a major environmental cue for human circadian regulation. Under visual-quality constraints, daylight-related spectral approximation and control of non-visual biological effects form a challenging multi-objective trade-off. This study proposes a hardware-explicit computational framework for circadian-oriented spectral optimization using five-channel LED basis spectra characterized from discrete SPD data. The framework integrates static scenario-constrained spectral optimization, time-series daylight-emulation analysis, and exploratory sleep-outcome characterization. The static model generates implementable spectra for fixed daytime and nighttime scenarios, while the time-series model evaluates the ability of the same LED basis to approximate daylight-related temporal characteristics. Sleep outcomes are analyzed from available repeated-measures data collected under static nighttime conditions: conventional lighting, darkness, and a predefined reference optimized nighttime condition derived from the static scenario. In a small-sample exploratory analysis (n = 11), the optimized condition showed a significant N3% difference relative to darkness (p = 0.03, |d| = 0.97), and the comparison with conventional lighting and most other sleep endpoints did not reach statistical significance. These findings suggest condition-associated variation in sleep architecture within the present dataset and provide exploratory evidence for hypothesis generation. Overall, the proposed framework offers a reproducible route for multi-channel LED spectral trade-off design, daylight-emulation assessment, and preliminary sleep-outcome characterization in circadian-oriented healthy-lighting applications.

KEYWORDS

TOPSIS-entropy weight method, differential evolution, SLSQP, time series constrained optimization, spectral optimization

INTRODUCTION

Solid-state lighting based on light-emitting diodes (LEDs) has become the dominant technology for indoor illumination owing to its high luminous efficacy, long service life, compact form, and spectral tunability. Beyond enabling visual perception, light also exerts pronounced non-visual effects on human physiology through retinal pathways involved in circadian entrainment, melatonin regulation, alertness, and sleep-related processes [1-3]. In particular, the spectral composition, intensity, duration, and timing of light exposure jointly determine circadian-relevant responses, making spectrum design a central issue in healthy indoor lighting [2-3].

The physiological basis of these non-visual effects was established by the discovery of intrinsically photosensitive retinal ganglion cells (ipRGCs) and by experimental evidence showing that short-wavelength light is especially effective in modulating melatonin and circadian responses [1]. On this foundation, contemporary lighting research has moved from qualitative descriptions of “blue-rich” or “warm” light toward quantitative circadian metrology and application-oriented spectral design. Recent reviews and expert recommendations consistently emphasize a “bright days, dim evenings” principle, namely, providing sufficiently strong circadian-effective light during the daytime while reducing circadian stimulation in the evening and at night to better support physiology, sleep, and wakefulness [2-3]. In this context, the CIE α-opic framework has enabled a more standardized evaluation of non-visual light effects. In the present study, circadian-relevant spectral performance is characterized primarily by melanopic daylight efficacy ratio (mel-DER), which quantifies melanopic effectiveness relative to photopic illuminance and is therefore well suited for spectrum-level comparison and optimization.

At the engineering level, circadian-oriented lighting design must satisfy not only physiological considerations but also visual-quality requirements and practical implementation constraints. For multi-channel LED systems, reducing circadian stimulation alone is insufficient if the resulting spectrum produces unacceptable color rendering, chromaticity deviation, or poor visual usability. Accordingly, standardized visual metrics such as the TM-30 color fidelity index (Rf) and gamut index (Rg) provide an important basis for evaluating spectral trade-offs in practical lighting design [4]. Meanwhile, recent studies have shown that dynamic daylight-like lighting and melanopic-aware spectral control can affect circadian rhythm, cognition, mood, melatonin timing, and alertness in real or quasi-real application settings, including closed environments, office spaces, and display-lighting scenarios [5-9]. These studies collectively indicate that properly designed time-varying

spectra may improve the physiological appropriateness of indoor lighting without necessarily sacrificing visual performance.

Despite this progress, several gaps remain between current circadian-lighting knowledge and deployable engineering methods. First, circadian metrics and visual-quality metrics are still often treated separately, whereas practical LED spectrum synthesis requires a unified framework that simultaneously accounts for circadian effectiveness, color quality, chromaticity control, and channel feasibility [2,4]. Second, many existing studies focus on static day/night lighting conditions, while deployable healthy-lighting systems also require methods for evaluating daylight-related temporal transitions under constrained LED channel configurations [5,7,9,10]. Third, manufacturability constraints, such as nonnegative channel weights, bounded drive signals, target chromaticity windows, and minimum color-quality thresholds, are not always modeled explicitly, which limits reproducibility and transferability across different multi-channel LED platforms [4,9,10]. Finally, improvements in circadian-related optical metrics do not necessarily translate directly into better sleep outcomes, and the physiological validity of a given spectral strategy still requires empirical verification under controlled conditions [3,6,8,11].

To address these issues, this paper proposes a hardware-explicit computational framework for circadian-oriented multi-channel LED spectral optimization. The framework is organized into four connected components. First, a unified metric-computation pipeline is established for visual and circadian-relevant indicators, including correlated color temperature (CCT), distance from the Planckian locus (Duv), TM-30 color fidelity and gamut indices (Rf and Rg), and melanopic daylight efficacy ratio (mel-DER). Second, a static scenario-constrained optimization model is formulated for representative daytime and nighttime lighting scenarios, with scenario-specific objective functions and engineering constraints. Third, a time-series constrained spectral matching model is developed to evaluate the daylight-emulation capability of the same five-channel LED system. Finally, sleep data collected under conventional lighting, darkness, and a predefined reference optimized nighttime lighting condition are analyzed through repeated-measures statistics and composite evaluation. The resulting framework links spectral metric calculation, scenario-oriented static design, daylight-emulation assessment, and exploratory sleep-outcome characterization within a common five-channel LED platform.

MODEL

LED Basis Spectra and Hardware Characterization for the Multi-Channel LED Source

The description of LED basis spectra and hardware characterization

The optimization models in this study are built on five empirical LED basis spectra, including blue, green, red, warm-white, and cold-white channels. The spectral power distribution (SPD) of each channel was obtained from the provided appendix dataset and was used directly as a discrete wavelength-dependent input. The SPD data were sampled from 380 to 780 nm at a 1 nm interval. Since the optimized channel weights are determined by the spectral characteristics of these basis spectra, the hardware characteristics of the five LED channels need to be explicitly reported before constructing the spectral optimization models. Therefore, the reproducibility claimed in this study refers to the reproducibility of the computational procedure under explicitly specified empirical LED basis spectra, rather than the transferability of identical numerical channel weights across arbitrary LED hardware.

The calculation of LED channel spectral characteristic parameters

For each LED channel, the discrete SPD vector is expressed as:

$$s_i = [S_i(\lambda_1), S_i(\lambda_2), ..., S_i(\lambda_N)]^T, i = 1, 2, ..., 5 \quad (1)$$

where $S_i(\lambda_j)$ denotes the relative spectral power of the i -th LED channel at wavelength λ_j , with λ_j ∈[380,780] nm and Δλ=1 nm.

The peak wavelength of each channel is defined as:

$$\lambda_{peak,i} = \arg\max_{\lambda \in \Lambda} S_i(\lambda). \quad (2)$$

The half-maximum value is calculated as:

$$H_i = 0.5 \times \max_{\lambda \in \Lambda} S_i(\lambda). \quad (3)$$

The full width at half maximum (FWHM) is defined as:

$$FWHM_i = \lambda_{R,i} - \lambda_{L,i}, \quad (4)$$

$$S_i(\lambda_{L,i}) = S_i(\lambda_{R,i}) = H_i. \tag{5}$$

Since the SPD data are discretely sampled at 1 nm intervals, the half-maximum crossing wavelengths are obtained by linear interpolation between adjacent samples:

$$\lambda^* = \lambda_a + \frac{H_i - S_i(\lambda_a)}{S_i(\lambda_b) - S_i(\lambda_a)}(\lambda_b - \lambda_a), \tag{6}$$

where λ_a and λ_b are two adjacent sampled wavelengths surrounding the half-maximum crossing. Based on the above definitions, the calculated spectral characteristics of the five LED channels are summarized in Table 1.

Table 1. Spectral characteristics of the five LED basis channels used in this study

Channel	Appendix column	Emission type	λ_{peak} / nm	Half-maximum interval / nm	FWHM / nm	SPD sampling range / nm	Sampling interval	Nominal CCT / K
Blue	Blue	Narrow-band blue	429.00	420.15–439.08	18.93	380–780	1 nm	—
Green	Green	Narrow-band green	521.00	506.17–541.74	35.57	380–780	1 nm	—
Red	Red	Narrow-band red	621.00	610.91–630.00	19.09	380–780	1 nm	—
Warm White	Warm White	Phosphor-converted warm white	618.00	555.57–682.41	126.84	380–780	1 nm	≈3000
Cold White	Cold White	Phosphor-converted cool white	456.00	447.15–467.95	20.80	380–780	1 nm	≈6500

λ_{peak} denotes the wavelength corresponding to the maximum relative spectral power. FWHM was calculated from the half-maximum interval around the dominant peak using linear interpolation between adjacent 1 nm samples. For phosphor-converted white channels, the reported FWHM characterizes the dominant half-maximum interval; the full discrete SPD data are used as model inputs because white LED spectra contain broadband phosphor-emission components.The subsequent modeling sections are developed on the same five-channel LED basis spectra and spectral metric system. The static scenario-constrained optimization model focuses on implementable spectral design under fixed daytime and nighttime lighting requirements. The time-series constrained spectral matching model extends the same spectral synthesis procedure to time-indexed

daylight targets and evaluates temporal daylight-emulation capability under the constrained LED basis. The sleep-related outcome analysis uses available repeated-measures data collected under conventional lighting, darkness, and a predefined reference optimized nighttime lighting condition to characterize condition-associated differences in objective sleep indicators. Together, these modules form a unified workflow covering spectral design, temporal daylight-emulation assessment, and preliminary sleep-outcome characterization.

Static Scenario-Constrained Optimization Model for a Multi-Channel LED Light Source

The description of static scenario-constrained optimization model for a multi-channel LED light source

This study establishes a static scenario-constrained optimization model for fixed lighting scenarios with predefined visual and circadian requirements [12]. Based on the five empirical LED basis spectra characterized in Table 1, including red, green, blue, warm-white, and cold-white channels, the model generates target spectral compositions by adjusting the corresponding channel weights. For daytime high-efficiency lighting, the optimization emphasizes color quality, daylight-like chromaticity, and sufficient melanopic stimulation. For nighttime low-circadian-stimulation lighting, the optimization emphasizes reduced mel-DER under minimum visual-usability constraints. For daytime high-efficiency lighting, the optimization emphasizes color quality, daylight-like chromaticity, and sufficient circadian stimulation. For nighttime low-circadian-stimulation lighting, the optimization emphasizes reduced mel-DER under minimum visual-usability constraints. The resulting formulation is a constrained nonlinear optimization problem with scenario-dependent objective functions and shared engineering constraints.

From an engineering perspective, this model serves as a static spectral design framework. For daytime high-efficiency lighting, it emphasizes color quality and visual comfort; for nighttime low-circadian-stimulation scenario, it emphasizes reduction of melanopic stimulation while maintaining basic color discrimination capability.

The establishment of static scenario-constrained optimization model for a multi-channel LED light source

The model is based on the physical additivity of optical spectra. When the emissions of multiple independent LED channels are mixed, the spectral radiant power at each wavelength can be regarded as the sum of the contributions from each channel. Let $S_i(\lambda)$ denote the normalized spectral power distribution of the i -th LED channel at wavelength λ , and let w_i denote its driving weight. Then the synthesized spectrum $\hat{S}(\lambda)$ is expressed as

$$\hat{S}(\lambda) = \sum_{i=1}^{5} w_i S_i(\lambda). \tag{7}$$

where, w_i represents the relative contribution of the i -th channel to the synthesized spectrum.

To give the weights clear physical meaning, each LED channel spectrum must first be normalized. Let $S_i^{(0)}(\lambda)$ denote the original spectrum of the i -th channel. Then the normalized spectrum can be written as

$$S_i(\lambda) = \frac{S_i^{(0)}(\lambda)}{\int_{\lambda_{\min}}^{\lambda_{\max}} S_i^{(0)}(\lambda)\, d\lambda}. \tag{8}$$

In the discrete case, the integral is approximated by summation over wavelength samples. This normalization removes dimensional inconsistency and original intensity differences, so that the weights directly represent the relative contribution of each channel under a common energy baseline.

The feasible region of the model is defined by two basic constraints. The first is the nonnegativity constraint:

$$w_i \geq 0, i = 1, 2, ..., 5. \tag{9}$$

This reflects the physical fact that LED driving currents cannot be negative. The second is the normalization constraint:

$$\sum_{i=1}^{5} w_i = 1. \tag{10}$$

This ensures a unified energy reference among different weight combinations and makes the optimization results comparable and practically implementable.

In static spectral design, the objective function is scenario-dependent rather than fixed. Therefore, the same multi-channel mixing framework is adapted to different application goals by changing the objective function and the associated constraints.

For the daytime high-efficiency lighting scenario, the design focus is high color quality and daylight-like color temperature. Therefore, the primary objective is to maximize the color fidelity index R_f : $\max R_f(\hat{S})$.

At the same time, correlated color temperature and color naturalness constraints are imposed. For example, to maintain daylight-like white light, the CCT can be constrained as

$$5500\ \mathrm{K} \leq \mathrm{CCT}\ (\hat{S}) \leq 6500\ \mathrm{K}, \tag{11}$$

Additional constraints are imposed on Rg and Duv to ensure natural color appearance without obvious chromatic deviation.

For the nighttime sleep-support lighting scenario, the design focus shifts from maximizing color quality to minimizing circadian disruption. Therefore, the primary objective becomes minimization of melanopic daylight efficacy ratio: $\min \text{mel-DER}\ (\hat{S})$.

At the same time, warm color temperature constraints and minimum color-quality constraints are imposed to avoid an excessively dim or visually unusable light source. For example,

$$2500\ \mathrm{K} \leq \mathrm{CCT}\ (\hat{S}) \leq 3500\ \mathrm{K} \tag{12}$$

together with minimum color-rendering constraints, ensures a balance between low melanopic stimulation and acceptable visual performance.

Thus, the general form of the static scenario-constrained optimization model can be written as

$$\min / \max_{w_i} f(\hat{S}) \tag{13}$$

$$\begin{aligned} s.t.\quad & \hat{S}(\lambda) = \sum_{i=1}^{5} w_i S_i(\lambda), \\ & w_i \geq 0, i = 1, 2, ..., 5, \\ & \sum_{i=1}^{5} w_i = 1, \\ & g_j(\hat{S}) \leq 0, j = 1, 2, ..., m, \end{aligned} \tag{14}$$

where $f(\hat{S})$ is the scenario-specific primary objective, such as maximizing R_f or minimizing mel-DER, and $g_j(\hat{S})$ represents the associated performance constraints on CCT, R_f , D_{uv} , and minimum visual quality. This

formulation allows the same hardware framework to support multiple lighting applications simply by changing the objective and constraint set.

Since the color-quality indices and circadian-related metrics are nonlinear functions of the synthesized spectrum, the established static scenario optimization model belongs to the class of constrained nonlinear optimization problems. To improve solution stability and applicability, both an SLSQP-based local constrained optimization method and a differential-evolution-based global optimization method are employed. The former is suitable for problems with locally smooth objective functions and explicit constraints, and can rapidly obtain feasible local optima, whereas the latter explores a broader solution space through population evolution and is more suitable for multimodal or non-convex problems. The combination of these two methods provides complementary solution paths for spectral optimization under different lighting scenarios.

Time-series Constrained Optimization Model for Dynamic Spectral Matching

The description of time-series constrained optimization model for dynamic spectral matching

To evaluate the temporal spectral-control capability of the five-channel LED system, this study constructs a time-series constrained spectral matching model [13-14]. The target inputs are time-indexed daylight spectra, and the decision variables include the normalized LED channel weights and an overall spectral scaling coefficient at each time point.

Based on the five empirical LED basis spectra characterized in Table 1, the synthesized spectrum is optimized to approximate selected daylight-related characteristics, including spectral shape, CCT, Rf, and mel-DER. The objective function combines wavelength-level spectral error with key-parameter deviations, so that the resulting time series reflects both physical spectral similarity and circadian-relevant metric consistency.

Functionally, this model evaluates the extent to which the constrained five-channel LED basis can approximate daylight-related temporal changes at the selected spectral and parameter levels. The generated sequence describes a controllable daylight-emulation strategy characterized by lower morning/evening CCT, higher daytime CCT, stable color fidelity, and time-varying melanopic effectiveness. The workflow of the proposed model is presented in Figure 1.

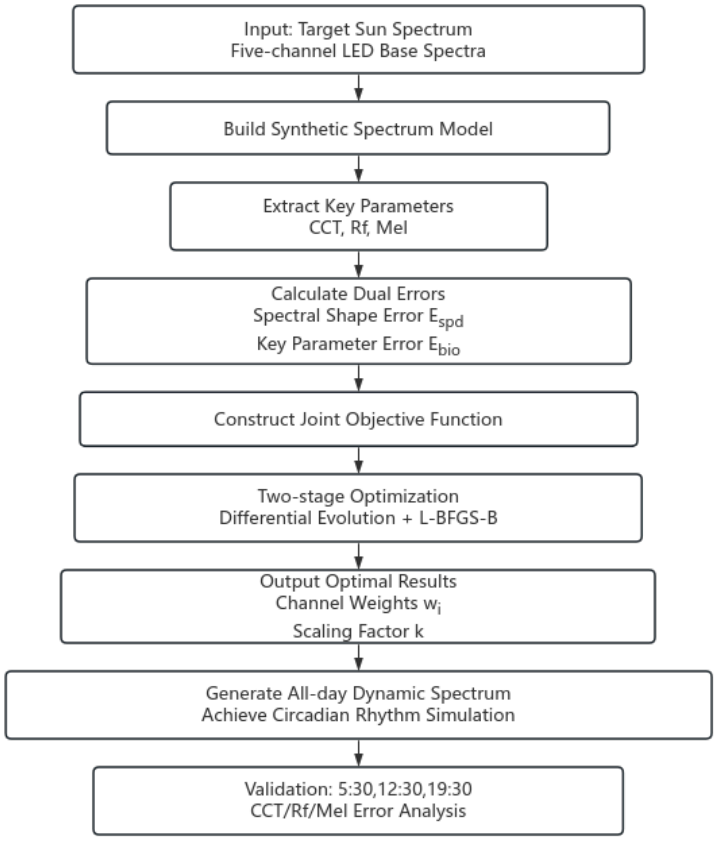

Figure 1. Workflow of the time-series constrained spectral matching model

As shown in Figure 1, the model takes the target daylight spectra and the five-channel LED basis spectra as inputs. The synthesized spectrum is constructed through weighted spectral superposition and spectral scaling. The optimization then evaluates wavelength-level spectral error and key-parameter deviations under channel-weight and scaling-coefficient constraints. Solving this problem at each time point generates a time-indexed lighting strategy for approximating selected daylight-related spectral, colorimetric, and melanopic metrics.

The establishment of time-series constrained optimization model for dynamic spectral matching

To model daylight-related temporal spectral approximation using a five-channel LED system, the synthesized spectrum at time t is represented as a weighted linear combination of the LED basis spectra, with an additional spectral scaling coefficient introduced to describe the overall energy level. Let $S_i(\lambda)$ denote the spectral power distribution of the i -th LED channel at wavelength λ , let $S_{sun}(\lambda, t)$ denote the target solar spectrum at time t , and let $\hat{S}(\lambda, t)$ denote the synthesized spectrum. Then the synthesized spectrum is expressed as follows:

$$\hat{S}(\lambda,t)=k_t\sum_{i=1}^{5}w_i(t)S_i(\lambda), \tag{15}$$

where $w_i(t)$ denotes the weight of the i -th LED channel at time t , representing its relative contribution to the synthesized spectrum, and k_t denotes the spectral intensity scaling coefficient at time t , which adjusts the overall amplitude of the synthesized spectrum so that it matches the total energy level of the target solar spectrum.

To ensure consistency between the synthesized spectrum and the target solar spectrum in both spectral shape and key photobiological parameters, this study establishes a joint error model composed of spectral shape error and key-parameter error. The former is used to characterize the overall discrepancy in spectral power distribution between the synthesized spectrum and the target solar spectrum, while the latter is used to measure deviations in key indicators such as CCT, Rf, and mel-DER. By jointly optimizing these error terms, the synthesized spectrum can approximate the target solar spectrum in multiple dimensions.

(1) Spectral shape error model

To quantify the discrepancy between the synthesized spectrum $\hat{S}(\lambda,t)$ and the target solar spectrum $S_{sun}(\lambda,t)$ across wavelengths, the spectral shape error is defined as

$$E_{spd}(t)=\sum_{\lambda}\omega(\lambda)[\hat{S}(\lambda,t)-S_{sun}(\lambda,t)]^2, \tag{16}$$

where $\omega(\lambda)$ is a wavelength-dependent weighting function that assigns different importance to different spectral regions.

(2) Key-parameter error model

A close match in spectral waveform alone does not guarantee equivalence in color rendering performance or physiological regulation effects. Therefore, an additional key-parameter error term is introduced to measure the deviations between the synthesized spectrum and the solar spectrum in correlated color temperature, color fidelity index, and melanopic ratio. It is defined as

$$E_{bio}(t)=\alpha_1\left(\frac{\widehat{\mathrm{CCT}}(t)-\mathrm{CCT}_{sun}(t)}{\mathrm{CCT}_{sun}(t)}\right)^2+\alpha_2\left(\frac{\widehat{R}_f(t)-R_{f,sun}(t)}{R_{f,sun}(t)}\right)^2+\alpha_3\left(\frac{\widehat{\mathrm{Mel}}(t)-\mathrm{Mel}_{sun}(t)}{\mathrm{Mel}_{sun}(t)}\right)^2 \tag{17}$$

where $\widehat{\mathrm{CCT}}(t)$, $\widehat{R}_f(t)$, and $\widehat{\mathrm{Mel}}(t)$ denote the correlated color temperature, color fidelity index, and melanopic indicator of the synthesized spectrum at time t , respectively; $\mathrm{CCT}_{sun}(t)$, $R_{f,sun}(t)$, and $\mathrm{Mel}_{sun}(t)$ denote the corresponding values of the target solar spectrum; and α_1 , α_2 , α_3 are weighting coefficients for the parameter errors [4,15].

(3) Joint objective error

To simultaneously account for spectral waveform fitting accuracy and key photobiological parameter matching, this study formulates a weighted objective function composed of the spectral shape error and the key-parameter error:

$$J(t) = \beta_1 E_{spd}(t) + \beta_2 E_{bio}(t), \tag{18}$$

and minimizes this function as the optimization objective: $\min J(t)$.

where β_1 and β_2 denote the weighting coefficients associated with the spectral shape error term and the key-parameter error term, respectively, and are used to regulate the contribution of the two types of errors in the overall optimization process.

To ensure physical feasibility and engineering applicability, the time-series spectral matching model is subject to the following constraints. First, the weights of all LED channels must be nonnegative:

$$w_i(t) \geq 0, i = 1, 2, ..., 5. \tag{19}$$

This constraint reflects the physical fact that LED driving weights cannot be negative. Second, in order for the channel weights to represent relative spectral contributions and to avoid arbitrary amplification or reduction of the entire weight vector, the weights are required to satisfy the normalization condition

$$\sum_{i=1}^{5} w_i(t) = 1. \tag{20}$$

In addition, the spectral intensity scaling coefficient must satisfy $k_t > 0$.

This constraint guarantees that the overall radiation intensity of the synthesized spectrum remains positive, which is consistent with the output characteristics of real lighting systems. Therefore, the feasible region of the model is jointly defined by three types of constraints: nonnegativity of the weights, normalization of the

weights, and positivity of the scaling coefficient. These constraints ensure that the optimization results are both physically meaningful and practically implementable in a multi-channel LED healthy lighting system. Accordingly, at any time t , the dynamic spectral matching model can be formulated as the following time-series constrained optimization problem:

$$\min_{w_i(t),k_t} J(t) = \beta_1 E_{spd}(t) + \beta_2 E_{bio}(t) \tag{21}$$

$$\begin{aligned} s.t. \quad & \hat{S}(\lambda,t) = k_t \sum_{i=1}^{5} w_i(t) S_i(\lambda), \\ & w_i(t) \geq 0, i = 1,2,...,5, \\ & \sum_{i=1}^{5} w_i(t) = 1, \\ & k_t > 0. \end{aligned} \tag{22}$$

where, $\hat{S}(\lambda,t)$ denotes the synthesized spectrum at time t , $S_i(\lambda)$ denotes the basis spectrum of the i -th LED channel, $w_i(t)$ denotes the corresponding channel weight at time t , and k_t denotes the spectral intensity scaling coefficient.

Statistical Evaluation of Sleep-Related Outcomes and Entropy-Weighted TOPSIS Comprehensive Assessment

The description of statistical evaluation of sleep-related outcomes and entropy weight-TOPSIS comprehensive evaluation model

To quantitatively compare sleep-related outcomes under different nighttime lighting conditions, this study establishes a statistical evaluation model combined with an entropy-weighted TOPSIS comprehensive assessment framework. Based on sleep monitoring data collected under different lighting environments, the model extracts six objective sleep indicators, including total sleep time, sleep efficiency, sleep onset latency, proportion of N3 sleep, proportion of REM sleep, and the number of awakenings after sleep onset, and then performs multi-level comparison and comprehensive evaluation of sleep quality across different lighting conditions [16-17].

The framework consists of two parts. The first is a statistical evaluation module based on a repeated-measures design, which is used to determine whether each sleep indicator differs significantly across lighting

conditions. The second is an entropy-weighted TOPSIS module, which is used to assign objective weights to multiple indicators and generate an overall ranking of sleep quality under different lighting environments. The former identifies changes in specific sleep phenotypes, whereas the latter characterizes overall sleep quality from a multidimensional perspective. Together, these two components enable systematic comparison of lighting-associated sleep differences from the perspectives of single-indicator significance and multi-indicator comprehensive performance.

This module provides a statistical and composite evaluation of sleep-related outcomes under conventional lighting, darkness, and a predefined reference optimized nighttime lighting condition. In the benchmark structure, darkness serves as a low-exposure physiological reference, and conventional lighting serves as the practical active-lighting comparator. The analysis characterizes lighting-associated differences in sleep architecture and comprehensive sleep indicators within the current repeated-measures dataset.

The establishment of statistical evaluation of sleep-related outcomes and entropy weight-TOPSIS comprehensive evaluation model

To characterize sleep quality under different lighting conditions, six objective sleep indicators are extracted from the sleep-stage recordings: total sleep time (TST), sleep efficiency (SE), sleep onset latency (SOL), proportion of N3 sleep (N3%), proportion of REM sleep (REM%), and the number of awakenings after sleep onset (NOA).

Let T_{N1} , T_{N2} , T_{N3} , and T_{REM} denote the durations of the N1, N2, N3, and REM stages, respectively, and let T_{record} denote the total recording duration. Then total sleep time is defined as

$$\mathrm{TST} = T_{N1} + T_{N2} + T_{N3} + T_{REM}. \tag{23}$$

This indicator reflects the actual amount of sleep obtained during the entire sleep period and serves as a basic measure of sleep quantity.

Sleep efficiency is defined as the ratio of total sleep time to total recording duration:

$$SE = \frac{\mathrm{TST}}{T_{record}}. \tag{24}$$

This indicator reflects the proportion of time in bed that is effectively converted into sleep and is an important measure of sleep continuity and stability.

Sleep onset latency represents the time interval from the beginning of recording to the first onset of sleep. Let $T_{sleeponset}$ denote the time of first sleep onset and T_{start} denote the beginning of recording. Then sleep onset latency is defined as

$$\mathrm{SOL} = T_{sleeponset} - T_{start}. \tag{25}$$

This metric characterizes how easily the subject falls asleep; a smaller value generally indicates a smoother transition into sleep.

The proportion of N3 sleep is defined as the fraction of N3-stage duration in total sleep time:

$$\mathrm{N3\%} = \frac{T_{N3}}{\mathrm{TST}}. \tag{26}$$

N3 sleep corresponds to slow-wave sleep and is an important marker of physiological recovery and deep sleep quality.

The proportion of REM sleep is defined as

$$\mathrm{REM\%} = \frac{T_{REM}}{\mathrm{TST}}. \tag{27}$$

This indicator is closely related to memory consolidation, cognitive processing, and emotional regulation.

The number of awakenings after sleep onset is used to quantify the frequency of sleep interruption after sleep has begun. It is defined as the total number of transitions from any sleep stage to wakefulness after sleep onset, denoted as

$$NOA = N_{wake}. \tag{28}$$

This indicator reflects the degree of sleep fragmentation, and smaller values usually indicate better sleep continuity.

Accordingly, the sleep quality of one subject under one lighting condition can be represented by the multidimensional indicator vector

$$Y = (\mathrm{TST}, \mathrm{SE}, \mathrm{SOL}, \mathrm{N3\%}, \mathrm{REM\%}, \mathrm{NOA}). \tag{29}$$

Among these indicators, TST, SE, N3%, and REM% are benefit-type indicators, for which larger values generally indicate better sleep quality, whereas SOL and NOA are cost-type indicators, for which smaller values are preferable. This directional distinction forms the basis of subsequent standardization and comprehensive evaluation.

Because each subject undergoes sleep monitoring under multiple lighting conditions, the data exhibit a typical repeated-measures structure. To ensure that the statistical procedures are consistent with the distributional characteristics of the sample, this study adopts a hierarchical workflow consisting of normality testing, variance-structure testing, and parametric or nonparametric significance testing.

First, each sleep indicator is tested for normality using the Shapiro–Wilk test. For indicators satisfying the normality assumption, Mauchly's test of sphericity is further conducted to determine whether the covariance structure satisfies the assumptions of repeated-measures ANOVA. If these conditions are met, repeated-measures ANOVA is employed to test whether the mean value of the indicator differs significantly across lighting conditions. If the assumptions for parametric testing are not satisfied, the Friedman test is used for nonparametric repeated-measures comparison.

In repeated-measures ANOVA, the test statistic is defined as

$$F = \frac{MS_{condition}}{MS_{error}}, \tag{30}$$

where $MS_{condition}$ denotes the mean square between lighting conditions and MS_{error} denotes the error mean square. This statistic is used to test whether the mean of a given sleep indicator differs significantly across lighting conditions.

For indicators that do not satisfy the assumptions for parametric testing, the Friedman statistic is written as

$$\chi_F^2 = \frac{12}{nk(k+1)} \sum_{j=1}^{k} R_j^2 - 3n(k+1), \tag{31}$$

where n is the number of subjects, k is the number of lighting conditions, and R_j is the rank sum under the j -th condition. This method does not require the data to follow a normal distribution and is suitable for small-sample repeated-measures data.

For indicators showing significant overall differences, post hoc pairwise comparisons are further performed, together with Bonferroni correction to control the accumulation of type-I error caused by multiple testing. In addition, to avoid relying exclusively on p -values, effect-size measures are introduced to quantify the practical magnitude of the differences. Cohen's d can be used for pairwise comparisons, while Kendall's W can be used to characterize the effect size of Friedman-test results.

The main purpose of this statistical evaluation module is first to determine whether different lighting conditions induce significant changes in specific sleep indicators, and then to evaluate the practical significance of such differences through effect-size measures. Compared with using a single comprehensive score alone, this approach is more sensitive to changes in key sleep phenotypes such as deep sleep proportion and sleep continuity.

Significance testing of individual sleep indicators can reveal local changes in sleep phenotypes under different lighting conditions, but it cannot directly answer the more comprehensive question of which lighting environment yields better overall sleep quality. To address this issue, this study further establishes an entropy-weighted TOPSIS comprehensive evaluation model to rank the overall sleep quality under different lighting conditions, thereby overcoming the limitations of single-indicator analysis in global assessment.

In the comprehensive evaluation stage, considering that the relationships between different sleep indicators and sleep quality are not always characterized by simple monotonic increase or decrease, total sleep time, sleep efficiency, sleep onset latency, the proportion of N3 sleep, the proportion of REM sleep, and the number of awakenings after sleep onset are all treated as interval-type indicators according to their physiological meanings, reference ranges of adult normal sleep architecture, and study-specific settings. The ideal intervals and their basis are listed in Table 2.

Table 2. Table of Ideal Ranges and Sources for Intermittent Sleep Indicators

Indicator	Ideal interval	Indicator type	Basis
Total sleep time (TST)	360–480 min	Interval-type	Study-specific setting + adult sleep-duration reference
Sleep efficiency (SE)	0.80–1.00	Interval-type	Common reference range in sleep-quality evaluation
Sleep onset latency (SOL)	10–20 min	Interval-type	Common reference range in sleep-study interpretation
Proportion of N3 sleep (N3%)	0.10–0.20	Interval-type	Common reference range of adult sleep architecture
Proportion of REM sleep (REM%)	0.20–0.25	Interval-type	Common reference range of adult sleep architecture
Number of awakenings after sleep onset (NOA)	0–2	Interval-type	Study-specific setting

Let the ideal interval of the j -th sleep indicator be [a_j, b_j], and let the raw observed value of the i -th evaluation object on this indicator be x_{ij} . The deviation distance is defined as

$$d_{ij} = \max(0, a_j - x_{ij}) + \max(0, x_{ij} - b_j). \tag{32}$$

The interval-type preprocessed value is then constructed as

$$x'_{ij} = -d_{ij}. \tag{33}$$

After the interval-type preprocessing, to eliminate differences in dimensions and value ranges among indicators, the transformed indicators are further standardized to form the standardized decision matrix

$$Z = (z_{ij})_{m \times n}, \tag{34}$$

where m denotes the number of evaluation objects and n denotes the number of evaluation indicators. Based on the standardized matrix, the proportion of the j -th indicator for the i -th evaluation object is defined as

$$p_{ij} = \frac{z_{ij}}{\sum_{i=1}^{m} z_{ij}}. \tag{35}$$

The entropy of the j -th indicator is then calculated as

$$e_j = -\frac{1}{\ln m} \sum_{i=1}^{m} p_{ij} \ln p_{ij}. \tag{36}$$

Accordingly, the information redundancy of the j -th indicator is

$$d_j = 1 - e_j. \tag{37}$$

The entropy weight of the j -th indicator is then obtained as

$$w_j = \frac{d_j}{\sum_{j=1}^{n} d_j}. \tag{38}$$

The essential idea of the entropy-weighting method is that an indicator with greater variation among evaluation objects contains more information and should therefore be assigned a larger objective weight.

After the indicator weights are determined, the weighted standardized matrix is constructed as

$$v_{ij} = w_j z_{ij}. \tag{39}$$

The positive ideal solution and negative ideal solution are then defined as

$$\mathbf{V}^{+} = \left\{ \max_i v_{ij} \right\}_{j=1}^{n}, \ \mathbf{V}^{-} = \left\{ \min_i v_{ij} \right\}_{j=1}^{n}. \tag{40}$$

The Euclidean distances from the i -th evaluation object to the positive and negative ideal solutions are respectively given by

$$D_i^{+} = \sqrt{\sum_{j=1}^{n} (v_{ij} - v_j^{+})^2}, D_i^{-} = \sqrt{\sum_{j=1}^{n} (v_{ij} - v_j^{-})^2}. \tag{41}$$

Finally, the relative closeness is defined as

$$C_i = \frac{D_i^{-}}{D_i^{+} + D_i^{-}}, 0 \le C_i \le 1. \tag{42}$$

A larger value of C_i indicates that the corresponding evaluation object is closer to the ideal optimal state, and therefore has better overall sleep quality. Based on this framework, the sleep quality under different lighting conditions can be comprehensively ranked, thereby complementing the local information provided by single-indicator analysis.

The entropy-weighted TOPSIS model operates by first assigning objective weights according to indicator dispersion and then ranking the candidate conditions according to their distances from the ideal solutions. Compared with single-indicator comparison methods, this model better captures the overall characteristics of sleep quality as a complex physiological phenotype; compared with subjective-weighting methods, it reduces

the bias caused by manually assigned weights. Therefore, it is well suited as a supplementary evaluation tool for the multi-indicator effects of lighting-intervention experiments

RESULTS AND ANALYSIS

The data used in this article comes from https://new.saikr.com/vse/chinamcm/2025.

Results and Analysis of Static Scenario-Constrained Optimization Model for a Multi-Channel LED Light Source

Optimization results for the daytime high-efficiency lighting scenario

This subsection employs the static scenario-constrained optimization model for multi-channel LED lighting to determine the spectral composition for the daytime high-efficiency lighting scenario. The objective is to obtain a synthesized spectrum with superior color quality and strong daytime stimulation under correlated color temperature and naturalness constraints. For this scenario, both a local constrained optimization strategy and a global heuristic optimization strategy were used to solve for the optimal channel weights, and the results are shown in Table 3.

Table 3. Daytime lighting scene results table

Method 1: Optimal LED Channel Weights		Parameter values	
Blue	0.0933	CCT	5500.0001
Green	0.1451	Duv	0.0078
Red	0.15	Rf	90.4774
Warm White	0.0334	Rg	99.2039
Cold White	0.5806	mel-DER	0.8314
Method 2: Optimal LED Channel Weights		Parameter values	
Blue	0.1508	CCT	5500.0200
Green	0.1703	Duv	−0.0061
Red	0.2408	Rf	92.8540
Warm White	0.0091	Rg	102.6510
Cold White	0.4289	mel-DER	0.8370

As shown in Table 3, under the local constrained optimization scheme, the synthesized spectrum is dominated by the cool-white channel, whose weight reaches 58.06%. The correlated color temperature is maintained at 5500 K, the color fidelity index R_f reaches 90.48, and mel-DER is 0.8314. These results indicate that, in the daytime scenario, a cool-white-dominated composition can effectively satisfy the requirement of a high color temperature while preserving high color quality and relatively strong circadian stimulation. Therefore, this

solution is well suited for lighting environments such as offices and study spaces, where alertness and visual discrimination are important.

In contrast, the global heuristic optimization scheme substantially increases the combined contribution of the three primary color channels, whose total proportion reaches 56.19%. The correlated color temperature remains at a comparable level, whereas R_f is further improved to 92.85 and mel-DER reaches 0.8370. This suggests that, under essentially the same correlated color temperature constraint, increasing the participation of the colored channels can further improve the color-rendering performance of the synthesized spectrum. In other words, the global optimization strategy does not substantially change the daytime color-temperature target, but achieves a better solution in terms of color quality by redistributing the channel composition.

A further comparison of the two solutions shows that the main difference between the two strategies in the daytime scenario does not lie in correlated color temperature, but in color quality and channel allocation. The local optimization scheme tends to rely more strongly on the cool-white channel to satisfy the constraints rapidly, whereas the global optimization scheme makes fuller use of the flexibility of multi-channel spectral mixing and achieves a better solution in terms of color-rendering performance. This indicates that the multi-channel LED system has strong spectral tuning potential in daytime scenarios, and that the optimum solution is not unique but depends on the balance between color-quality objectives and the search mechanism of the optimization strategy.

Optimization results for the nighttime sleep-support lighting scenario

This subsection uses the same static scenario-constrained optimization model to solve the spectral composition for the nighttime sleep-support lighting scenario. The goal here is to minimize melatonin suppression while preserving basic visual usability, thereby establishing a lighting environment better suited to relaxation and preparation for sleep. For this scenario, both the local constrained optimization strategy and the global heuristic optimization strategy were applied, and the results are shown in Table 4.

Table 4. Nighttime lighting scene results table

Method 1: Optimal LED Channel Weights		Parameter values	
Blue	0.0021	CCT	2500.0100
Green	0.0921	Duv	0.0030
Red	0.0989	Rf	91.8060
Warm White	0.8069	Rg	94.1810
Cold White	0	mel-DER	0.3901

Method 2: Optimal LED Channel Weights		Parameter values	
Blue	0	CCT	2500.0100
Green	0.0344	Duv	0.0009
Red	0	Rf	88.6970
Warm White	0.9656	Rg	98.3910
Cold White	0	mel-DER	0.3668

As shown in Table 4, for the nighttime scenario, both strategies stabilize the correlated color temperature at 2500 K, indicating that a warm low-color-temperature environment is the common optimal direction for this application. Under the local constrained optimization scheme, the synthesized spectrum achieves R_f =91.81 and mel-DER=0.3901. This shows that the solution can already substantially reduce circadian interference while still maintaining relatively high color quality, thereby balancing basic visual performance with sleep-supportive properties.

Under the global heuristic optimization scheme, the correlated color temperature remains at 2500 K, but mel-DER is further reduced to 0.3668 due to a lower contribution of blue-related channels. This indicates that the global solution is more advantageous in reducing melatonin suppression. At the same time, the color-rendering performance remains at a high level, suggesting that the globally optimized channel-weight allocation can exploit the tuning capacity of the multi-channel LED system more fully and achieve a better compromise between lower physiological stimulation and acceptable visual performance.

These results show that the nighttime sleep-support scenario differs substantially from the daytime high-efficiency lighting scenario in optimization direction. The former emphasizes the reduction of short-wavelength components and the control of physiological stimulation, whereas the latter emphasizes the coordinated realization of high color quality and a high-correlated-color-temperature environment. The static scenario-constrained optimization model is therefore able to generate differentiated spectral solutions for different functional objectives, demonstrating good scenario adaptability and engineering value.

Comparison and discussion of different solution strategies

Based on the results in Tables 3 and 4, the local constrained optimization strategy and the global heuristic optimization strategy exhibit relatively clear functional differences in the two scenarios. For the daytime high-efficiency lighting scenario, the local optimization scheme can rapidly obtain a feasible solution satisfying both color temperature and color-rendering requirements, whereas the global optimization scheme further improves color quality and demonstrates stronger color reproduction capability. For the nighttime sleep-support lighting scenario, both methods can stably achieve the low-color-temperature target, but the global

optimization scheme is more advantageous in reducing mel-DER, indicating that it is more capable of finding a better compromise when visual requirements and non-visual physiological requirements conflict strongly.

From an engineering perspective, the local constrained optimization strategy has the advantages of high computational efficiency and simpler implementation, and is therefore suitable for scenarios requiring rapid computation or practical deployment. In contrast, the global heuristic optimization strategy involves higher computational cost but performs better in the joint optimization of color quality and circadian-related effects, making it more suitable for offline spectral design or parameter calibration of high-performance healthy-lighting schemes. The comparison of these two strategies demonstrates that the static scenario-constrained optimization model can not only generate targeted optimal spectral compositions for different lighting objectives, but also allow the choice of solution strategy according to application needs, thereby balancing engineering feasibility with spectral performance.

Overall, the static scenario-constrained optimization model for multi-channel LED lighting shows good adaptability in both the daytime and nighttime scenarios. On the one hand, the results indicate that multi-channel spectral mixing can achieve targeted control of correlated color temperature, color quality, and circadian-related effects through weight reallocation. On the other hand, they show that this model can provide a reasonable static spectral-design basis for the subsequent dynamic spectral matching model, and can also offer practically implementable parameter references for scenario-specific spectral design in real healthy-lighting systems.

Results and Analysis of Time-Series Constrained Optimization Model for Dynamic Spectral Matching

Dynamic spectral matching results

In this subsection, the proposed model is employed to fit the target solar spectrum over the full daytime period, solve for the optimal five-channel LED weight combination and scaling coefficient at each time point, and evaluate the ability of the synthesized spectrum to track the target solar spectrum in terms of both spectral shape and key photobiological parameters.

The results are presented in Table 5. For different time points, the model outputs the corresponding channel weights, spectral scaling coefficient, and key parameters of the synthesized spectrum. The numerical channel weights reported in Table 5 are conditional on the five empirical LED basis spectra characterized in Table 1; for other LED packages or channel spectra, the same optimization workflow can be applied, but the channel weights should be recalculated. Table 5 shows that the normalized channel weights remain nearly unchanged

from 05:30 to 17:30, while the scaling coefficient k varies across this period. This indicates that, under the present five-channel LED basis and optimization constraints, daytime tracking is mainly achieved through intensity scaling rather than substantial redistribution of channel weights. More evident spectral-composition changes appear after 18:30, corresponding to the evening decrease in CCT and mel-DER.

Table 5. Optimization results of the proposed time-series model

Time	w1_norm	w2_norm	w3_norm	w4_norm	w5_norm
05:30	0.17	0.12	0.22	0.00	0.49
06:30	0.17	0.12	0.22	0.00	0.49
07:30	0.17	0.12	0.22	0.00	0.49
08:30	0.17	0.12	0.22	0.00	0.49
09:30	0.17	0.12	0.22	0.00	0.49
10:30	0.17	0.12	0.22	0.00	0.49
11:30	0.17	0.12	0.22	0.00	0.49
12:30	0.17	0.12	0.22	0.00	0.49
13:30	0.17	0.12	0.22	0.00	0.49
14:30	0.17	0.12	0.22	0.00	0.49
15:30	0.17	0.12	0.22	0.00	0.49
16:30	0.17	0.12	0.22	0.00	0.49
17:30	0.17	0.12	0.22	0.00	0.49
18:30	0.15	0.12	0.23	0.01	0.48
19:30	0.14	0.19	0.14	0.25	0.29
Time	k	CCT_mix	Rf_mix	Mel_mix	spec_rel_rmse
05:30	0.51	5655.63	92.28	0.86	0.54
06:30	0.50	5635.70	92.30	0.86	0.55
07:30	0.50	5635.73	92.29	0.86	0.55
08:30	0.49	5639.78	92.26	0.86	0.55
09:30	0.52	5649.63	92.29	0.86	0.54
10:30	0.55	5641.68	92.30	0.86	0.54
11:30	0.57	5625.82	92.28	0.86	0.54
12:30	0.61	5699.65	92.22	0.86	0.53
13:30	0.57	5623.86	92.27	0.86	0.54
14:30	0.54	5627.79	92.29	0.86	0.54
15:30	0.52	5635.71	92.29	0.86	0.54
16:30	0.49	5627.76	92.29	0.86	0.55
17:30	0.35	5619.88	92.26	0.86	0.57
18:30	0.20	5364.54	92.41	0.84	0.61
19:30	0.06	3887.53	93.44	0.64	0.70

At the selected-parameter level, the synthesized spectra show close agreement with the target daylight series in CCT, Rf, and mel-DER. Across all time points, the mean absolute error of CCT is 269.7 K, the mean absolute error of Rf is 6.58, and the mean relative error of mel-DER is 3.78%. These results indicate that the model captures the main temporal variation of the target daylight spectra in the selected colorimetric and melanopic indicators.

The spectral relative RMSE ranges from 0.53 to 0.70, showing that waveform-level reconstruction remains constrained by the finite number and spectral shapes of the five LED basis channels. Therefore, the dynamic model is more suitable for daylight-related parameter tracking and temporal spectral-control analysis than for exact solar-spectrum reconstruction.

A further examination of the representative time points in Table 5 shows that the synthesized spectra maintain CCT values above 5600 K and Rf values above 92 during most daytime hours. This indicates that the optimized spectra preserve a daylight-like chromatic appearance and high color fidelity within the feasible range of the five-channel LED system. During the evening transition, the CCT decreases from 5364.54 K at 18:30 to 3887.53 K at 19:30, accompanied by a reduction in mel-DER from 0.84 to 0.64. This coordinated decrease in CCT and melanopic effectiveness reflects the intended transition toward a lower-stimulation evening spectrum. Overall, the time-series solution captures the main “warm morning/evening–cool daytime” daylight pattern through joint adjustment of channel weights and spectral scaling.

Spectral comparison at representative time points

To verify the spectral reconstruction performance of the model at representative periods, the synthesized spectrum and the target solar spectrum were compared at three characteristic time points: morning, noon, and evening. The results are shown in Figure 2.

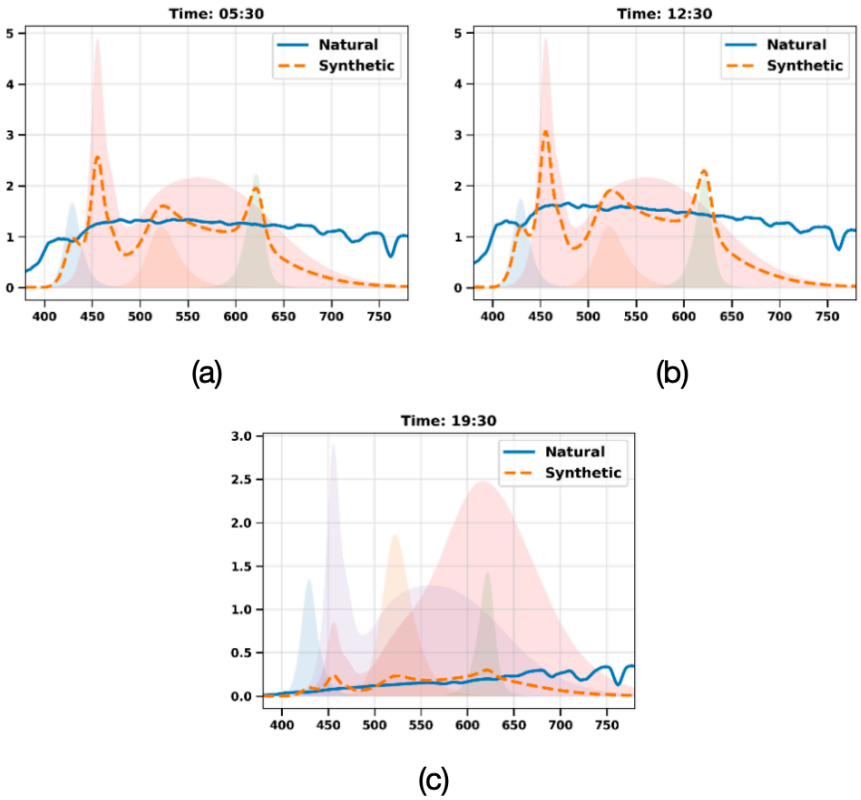

Figure 2. Comparison of the synthesized spectrum and the target solar spectrum: (a) Time 05:30; (b) Time 12:30; (c) Time 17:30

Figure 2 compares the synthesized spectra with the target solar spectra at three representative time points. The synthesized spectra capture the dominant spectral components that can be expressed by the five-channel LED basis, especially the short-wavelength peak associated with the blue channel and the long-wavelength contribution associated with the red and warm-white channels. At the morning and evening time points, the fitted spectra show relatively stronger long-wavelength components, corresponding to lower CCT values. At the noon time point, the fitted spectrum exhibits a stronger short-wavelength component and a more balanced visible-band distribution, corresponding to the higher CCT target.

These spectral comparisons indicate that the dynamic spectral matching model achieves feasible wavelength-level approximation within the spectral basis formed by the five LED channels. The remaining waveform discrepancy is mainly associated with the limited number of basis spectra and the fixed emission profiles of the LED channels. This observation highlights the need to evaluate both integrated metrics and wavelength-level spectral agreement when designing circadian-oriented multi-channel lighting systems.

Temporal variation of key parameters

In addition to the spectral-shape comparison, the temporal variation of the key parameters of the synthesized spectrum and the target solar spectrum was further compared over the full daytime period, as shown in Figure 3. This analysis focuses on the synchronization of three major indicators in time: correlated color temperature, color fidelity index, and mel-DER.

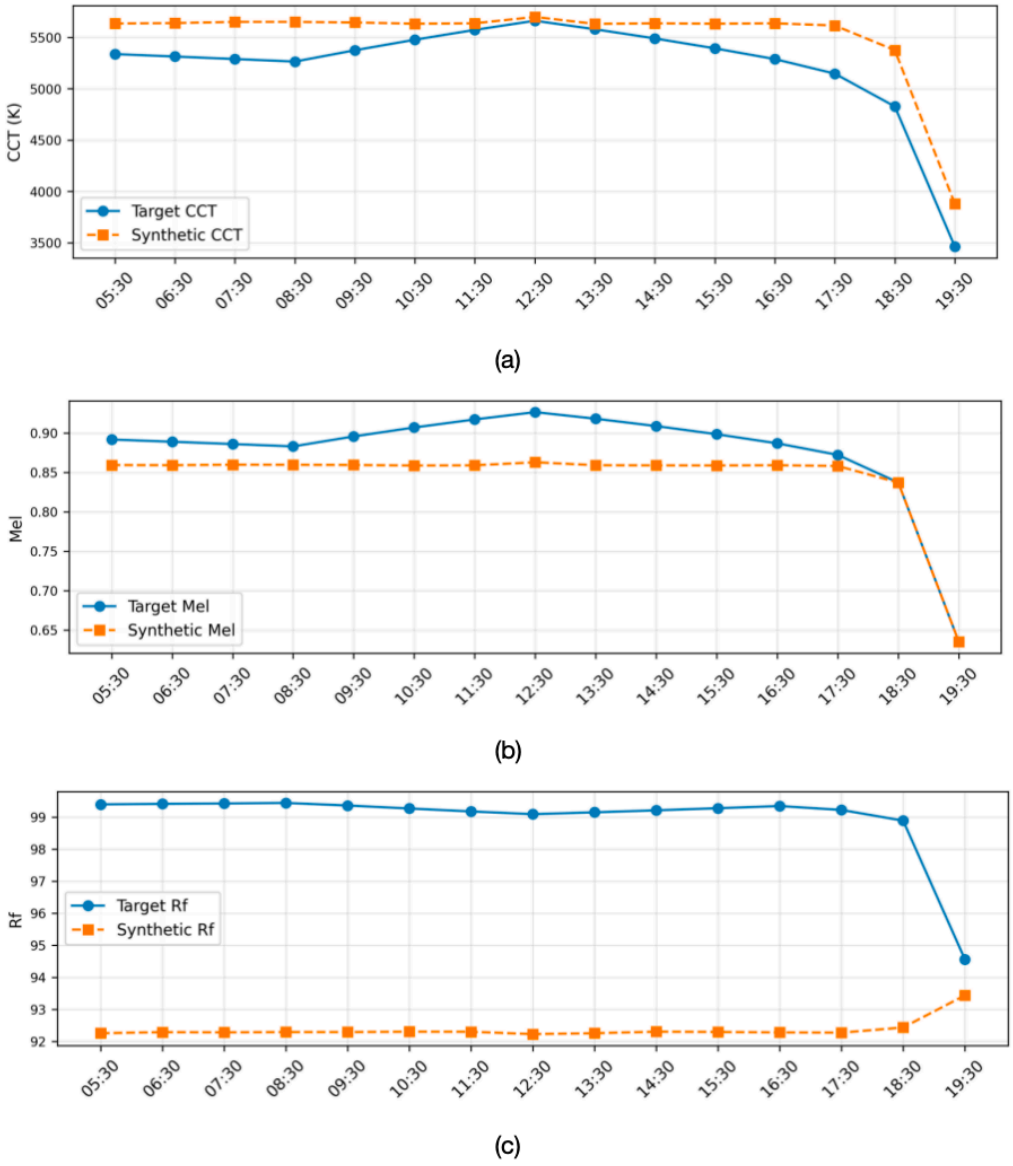

Figure 3. Comparison of core parameters between the synthesized spectrum and the target solar spectrum: (a) CCT; (b) Mel; (c) Rf

As shown in Figure 3, the CCT curve of the synthesized spectrum follows the same low–high–low temporal pattern as the target solar spectrum, with lower values during the morning and evening periods and higher values around midday. This trend confirms that the optimized time series preserves the main chromatic

transition of natural daylight at the parameter level. The Rf curve remains above 92 for most time points, indicating stable color fidelity during the dynamic matching process. Together, the CCT and Rf results show that the model maintains daylight-like chromatic variation while keeping the synthesized spectra within a high-fidelity color-rendering range.

The mel-DER curve of the synthesized spectrum follows the temporal variation of the target daylight series, indicating that the optimized spectra preserve the main melanopic trend across the day. Together with the spectral comparisons in Figure 2, the parameter curves in Figure 3 show that the proposed model coordinates wavelength-level fitting, colorimetric consistency, and melanopic-metric tracking within the constrained five-channel LED basis.

Discussion of results

Taken together, the results in Table 5, Figure 2, and Figure 3 show that the proposed model captures the main temporal transition of daylight-like lighting under the five-channel LED configuration. During most daytime points, the normalized channel weights remain stable, and the temporal variation is mainly represented by the spectral scaling coefficient k. This indicates that the daytime targets share a similar constrained spectral composition, with intensity modulation accounting for most of the time-dependent change. During the evening transition, the normalized channel composition changes more clearly, accompanied by lower CCT and reduced mel-DER. The resulting “warm morning/evening–cool daytime” pattern demonstrates the temporal control potential of the five-channel LED basis and provides a methodological reference for circadian-oriented dynamic lighting design.

Exploratory Analysis of Sleep-Related Outcomes and Entropy-Weighted TOPSIS Assessment

Distribution characteristics of sleep indicators and overall significance-test results

This subsection employs the statistical evaluation model of sleep-related outcomes to examine the overall differences in the six sleep indicators under the three lighting conditions, with the aim of identifying which sleep phenotypes are most sensitive to nighttime lighting variation. Based on the original indicator data of 11 subjects shown in Table 6, normality tests and repeated-measures statistical analyses were first performed, and the significance levels together with effect sizes were then used to interpret the characteristics of indicator variation.The data for the paper were obtained with the consent of the participants, who signed informed consent forms, and received ethical approval from Hunan Agricultural University.

Table 6. Parameters of various indicators of 11 subjects under three environments

Night 1						
Serial number	TST(min)	SE	SOL(min)	N3_percent	REM_percent	NumOfAwakenings
Subject 1	310	0.870	15	0.147	0.205	19
Subject 2	322	0.658	16	0.172	0.321	17
Subject 3	360.5	0.918	4	0.214	0.262	12
Subject 4	334	0.837	40.5	0.247	0.340	13
Subject 5	397.5	0.933	16	0.269	0.225	16
Subject 6	382.5	0.897	31	0.142	0.153	11
Subject 7	371	0.843	31	0.187	0.267	14
Subject 8	381.5	0.894	31	0.127	0.140	13
Subject 9	491	0.923	6.5	0.198	0.326	22
Subject 10	356	0.883	7	0.174	0.324	14
Subject 11	329.5	0.773	23.5	0.214	0.217	11
Night 2						
Serial number	TST(min)	SE	SOL(min)	N3_percent	REM_percent	NumOfAwakenings
Subject 1	312	0.900	2	0.245	0.232	19
Subject 2	348	0.752	5	0.309	0.297	13
Subject 3	260	0.713	51	0.281	0.202	14
Subject 4	386	0.944	13	0.202	0.424	11
Subject 5	430.5	0.940	16	0.094	0.361	15
Subject 6	358.5	0.746	75	0.109	0.218	12
Subject 7	401.5	0.883	47.5	0.202	0.280	8
Subject 8	375.5	0.885	2	0.226	0.208	17
Subject 9	455.5	0.934	13.5	0.202	0.290	25
Subject 10	453.5	0.964	5.5	0.108	0.268	11
Subject 11	389.5	0.961	8.5	0.155	0.171	11
Night 3						
Serial number	TST(min)	SE	SOL(min)	N3_percent	REM_percent	NumOfAwakenings
Subject 1	288.5	0.821	5	0.256	0.256	19
Subject 2	347	0.917	0	0.278	0.236	16
Subject 3	259	0.682	54.5	0.216	0.241	12
Subject 4	347	0.874	7	0.341	0.216	9
Subject 5	384	0.844	2	0.272	0.181	14
Subject 6	365	0.917	2.5	0.260	0.125	11
Subject 7	379.5	0.943	7	0.227	0.075	9
Subject 8	435	0.954	2	0.260	0.360	12
Subject 9	437	0.955	1.5	0.159	0.205	22
Subject 10	347	0.939	9	0.182	0.244	8
Subject 11	367.5	0.873	24	0.261	0.193197279	20

The overall significance-test results are shown in Table 7. Total sleep time (TST), sleep efficiency (SE), sleep onset latency (SOL), proportion of REM sleep (REM%), and the number of awakenings after sleep onset (NOA) show no statistically significant differences among the three lighting conditions, and their effect sizes remain relatively small. This pattern indicates limited between-condition separation for these indicators in the present dataset. In contrast, the proportion of N3 sleep (N3%) shows a statistically significant difference with a moderate-to-large effect size, suggesting that deep-sleep proportion provides the clearest sleep-structure signal among the six indicators.

Table 7. Significant difference results

metric	Way	normality	sphericity	p	η^2	W
TST(min)	RM-ANOVA	TRUE	TRUE	0.39	0.09	
SE	RM-ANOVA	TRUE	TRUE	0.73	0.03	
SOL(min)	Friedman	FALSE		0.31		0.11
N3_percent	RM-ANOVA	TRUE	TRUE	0.05	0.26	
REM_percent	RM-ANOVA	TRUE	TRUE	0.17	0.16	
NumOfAwakenings	Friedman	FALSE		0.17		0.16

These findings suggest that the sleep indicators show heterogeneous sensitivity to lighting conditions in the present dataset. Global measures such as total sleep time and sleep efficiency exhibit limited between-condition separation, whereas N3% shows a clearer condition-associated difference. Therefore, among the single indicators considered here, N3% provides the most informative sleep-structure signal for the current exploratory analysis.

Visual analysis of sleep-indicator distributions

To further illustrate the distributional differences of the sleep indicators across lighting conditions, boxplots of the six indicators were generated on the basis of the significance analysis, as shown in Figure 4. This subsection uses boxplot visualization to compare the medians, dispersion, and outlier distributions of the indicators under the three lighting conditions, thereby assisting in the interpretation of the statistical results.

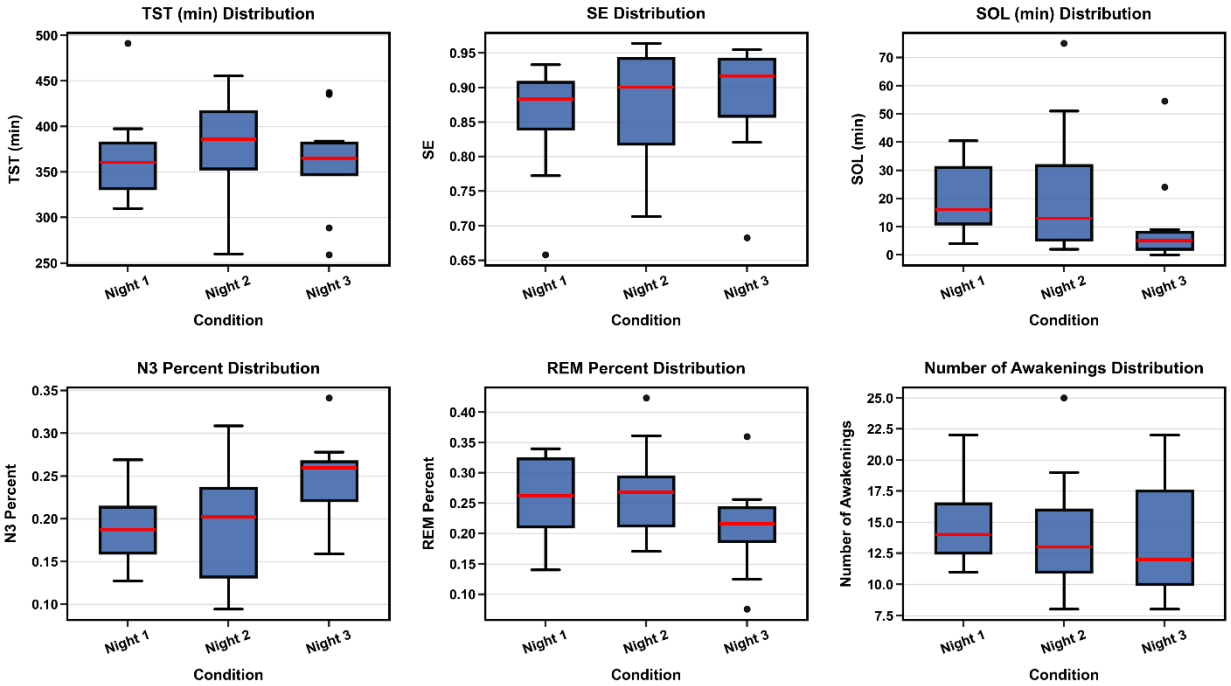

Figure 4. Indicator distribution box plot

As shown in Figure 4, the distribution ranges of TST, SE, SOL, and REM% are relatively similar across the three lighting conditions. The differences in median values are limited, and the degree of overlap among the boxes is substantial, indicating weak between-condition separation for these indicators under the present experimental setting. This pattern is consistent with the non-significant results reported in Table 7.

The boxplot of N3% shows a more visible separation among the three lighting conditions, especially between the predefined reference optimized lighting condition and darkness. This distributional pattern is consistent with the overall significance-test result for N3% in Table 7 and provides a visual basis for the subsequent pairwise comparison. Compared with total sleep time, sleep efficiency, and REM%, the N3% distribution presents a clearer sleep-architecture difference across lighting conditions in the present dataset.

Pairwise comparison analysis of N3-sleep proportion

Because the proportion of N3 sleep shows a significant overall difference in the preceding analysis, pairwise comparisons were further performed to identify the specific source of this difference among the predefined reference optimized lighting, conventional lighting, and darkness conditions. The results are presented in Table 8.

Table 8. Results of N3% significance differences under different environments

metric	pair	test	p_bonf	reject	effect_size_d
N3_percent	Night 1 vs Night 2	Paired t	1.00	FALSE	−0.04
N3_percent	Night 1 vs Night 3	Paired t	0.03	TRUE	−0.97
N3_percent	Night 2 vs Night 3	Paired t	0.18	FALSE	−0.63

As shown in Table 8, the difference in N3% between the predefined reference optimized lighting and conventional lighting is not statistically significant. The difference between the predefined reference optimized lighting and darkness is statistically significant, with a relatively large effect size. The comparison between conventional lighting and darkness also does not reach statistical significance. These results identify N3% as the sleep indicator showing the clearest condition-associated difference involving the predefined reference optimized lighting under the current sample condition. Darkness represents a low-exposure physiological reference, and conventional lighting represents the practical active-lighting comparator. Within this benchmark structure, the N3% result characterizes a sleep-structure difference associated with lighting condition.

From the perspective of sleep physiology, N3 sleep is a key component of slow-wave sleep and is closely related to physical recovery, neural restoration, and internal homeostatic regulation. In the present dataset, the observed N3% difference indicates a condition-associated change in sleep structure. Most other sleep endpoints show no statistically significant differences, indicating limited evidence for broad sleep-physiological changes under the current sample size and experimental conditions.

Results of comprehensive sleep-quality scores

On the basis of the single-indicator significance analysis, this study further employs the entropy-weighted TOPSIS comprehensive evaluation model to rank overall sleep quality under the three lighting conditions, thereby avoiding reliance on a single local indicator while neglecting the multidimensional nature of sleep quality. The model integrates the six indicators TST, SE, SOL, N3%, REM%, and NOA through objective weighting and ideal-solution distance evaluation to obtain a comprehensive sleep-quality score.

The comprehensive scores show that the mean sleep-quality scores under the predefined reference optimized lighting, conventional lighting, and darkness are 0.742614, 0.714242, and 0.697217, respectively. The predefined reference optimized lighting condition has the highest mean comprehensive score, followed by conventional lighting and darkness. From the perspective of multi-indicator integration, this result represents

a higher descriptive average score under the predefined reference optimized lighting condition in the current dataset.

To further examine the statistical significance of the comprehensive scores, the overall sleep-quality scores were subjected to significance testing. Because the score distribution does not satisfy the normality assumption, the Friedman test was used. The result yields p =0.529, indicating no statistically significant difference, and Kendall's W ≈0.0579, indicating a very small overall effect size. The higher mean comprehensive score under the predefined reference optimized lighting condition does not correspond to a statistically significant group-level difference under the current sample size and experimental conditions.

The single-indicator analysis and the entropy-weighted TOPSIS analysis provide complementary information. The former identifies N3% as the most condition-sensitive sleep indicator in the current dataset, and the latter summarizes the overall pattern across multiple sleep-related indicators. The comprehensive-score result shows a descriptive multi-indicator tendency, with no statistically significant group-level separation among the three lighting conditions.

General discussion of the results

Figure 5 shows the visual comparison of the comprehensive sleep-quality scores under the three lighting conditions. Combined with the results in Table 7, Table 8, and Figures 4–5, the observed differences among lighting conditions are mainly reflected in sleep-structure indicators. The predefined reference optimized lighting differs significantly from darkness in N3%, and its difference from conventional lighting is not statistically significant. The predefined reference optimized lighting yields the highest mean comprehensive score among the three conditions, with no statistically significant group-level difference in comprehensive scores.

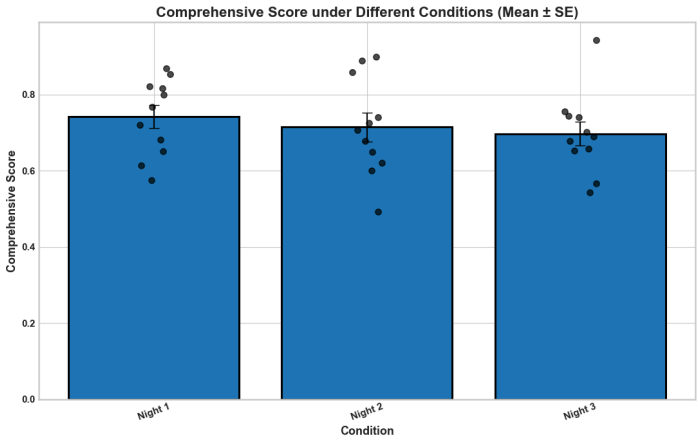

Figure 5. Comparison chart of N3% comprehensive score under different environments

From a methodological perspective, the statistical significance tests and the entropy-weighted TOPSIS comprehensive evaluation provide complementary perspectives in this part of the study. The former identifies which specific sleep phenotypes are sensitive to lighting variation, whereas the latter evaluates the overall effect of different lighting environments from a multidimensional point of view. These results indicate that the observed lighting-associated difference is concentrated mainly in N3%, while broader sleep-quality improvement is not supported by most individual endpoints in the current dataset.

From an application perspective, the proposed model provides a reproducible computational basis for designing nighttime lighting spectra with reduced mel-DER and basic visual usability. The current sleep-data analysis provides empirical context for comparing the predefined reference optimized lighting, conventional lighting, and darkness conditions. In future studies, matched active-lighting comparisons should be conducted under controlled illuminance, exposure duration, timing, and participant characteristics. Larger samples, more lighting-parameter combinations, and longer observation periods would further support the evaluation of stability and generalizability.

CONCLUSIONS AND OUTLOOKS

This study developed a hardware-explicit computational framework for circadian-oriented spectral design using a five-channel LED lighting system. The framework includes a common metric-computation pipeline, a static scenario-constrained optimization model, a time-series constrained daylight-emulation model, and an exploratory sleep-outcome analysis module.

The static scenario-constrained optimization results show that the five-channel LED system can generate differentiated spectra for daytime high-efficiency lighting and nighttime low-circadian-stimulation lighting through channel-weight adjustment. Under the daytime scenario, the optimized spectra maintained high color fidelity and daylight-like chromaticity. Under the nighttime scenario, the optimized spectra reduced mel-DER while preserving basic visual usability. These results demonstrate the feasibility of scenario-oriented spectral trade-off design under explicit engineering constraints.

The time-series constrained spectral matching results further indicate that the same LED basis can approximate the main temporal trend of daylight-related parameters. The synthesized spectra captured the representative warm morning/evening and cooler daytime transition pattern at the selected parameter level, although the finite number and spectral shapes of the LED basis channels limited full solar-spectrum recon-

struction. This result provides a methodological reference for dynamic daylight-emulation design based on constrained multi-channel LED sources.

In the exploratory sleep-outcome analysis, the predefined reference optimized nighttime lighting condition showed a significant N3% difference relative to darkness, while its difference from conventional lighting and most other sleep endpoints did not reach statistical significance. The entropy-weighted TOPSIS score was descriptively highest under the predefined reference optimized lighting condition, with no statistically significant group-level difference. These findings suggest lighting-associated variation in sleep architecture within the present dataset and provide preliminary evidence for subsequent larger-sample studies.

The main contribution of this study lies in linking spectral metric calculation, scenario-specific static optimization, dynamic daylight-emulation assessment, and preliminary sleep-outcome characterization within a reproducible five-channel LED framework. The reported LED basis spectra, spectral-characterization parameters, objective functions, constraints, and solver settings support computational reproducibility. Future work should include larger-sample studies, matched active-lighting comparisons, controlled illuminance and exposure timing, and longer observation periods. Further modeling should also incorporate spatial illuminance distribution, inter-individual physiological variability, and long-term user behavior.

Future work should focus on expanding the experimental sample and including more diverse populations to improve robustness. The dynamic model can be extended by incorporating environmental distribution, physiological feedback, and real-time adaptive control to form a closed-loop optimization framework. Long-term intervention studies are also needed to further verify the circadian and sleep-related effects of optimized lighting in practical applications.

Author Contributions

Conceptualization – Jinwang Luo; methodology – Jinwang Luo; formal analysis – Jinwang Luo; investigation – Jinwang Luo; writing-original draft preparation – Jinwang Luo; writing-review and editing – Jinwang Luo; visualization – Jinwang Luo; supervision – Jinwang Luo. All authors have read and agreed to the published version of the manuscript.

Conflicts of Interest

The author declares no conflict of interest.

Funding

This research received no external funding.

Acknowledgements

Not applicable.

REFERENCES

[1] Lucas RJ, Peirson SN, Berson DM, et al. Measuring and using light in the melanopsin age. Trends in neurosciences. 2014; 37(1): 1-9. doi: 10.1016/j.tins.2013.10.004

[2] Vetter C, Pattison PM, Houser K, et al. A review of human physiological responses to light: implications for the development of integrative lighting solutions. Leukos. 2022; 18(3): 387-414. doi: 10.1080/15502724.2021.1872383

[3] Brown TM, Brainard GC, Cajochen C, et al. Recommendations for daytime, evening, and nighttime indoor light exposure to best support physiology, sleep, and wakefulness in healthy adults. PLoS biology. 2022; 20(3): e3001571. doi: 10.1371/journal.pbio.3001571

[4] Royer MP. Tutorial: Background and guidance for using the ANSI/IES TM-30 method for evaluating light source color rendition. Leukos. 2022; 18(2): 191-231. doi: 10.1080/15502724.2020.1860771

[5] Nie J, Zhou T, Chen Z, et al. The effects of dynamic daylight-like light on the rhythm, cognition, and mood of irregular shift workers in closed environment. Scientific reports. 2021; 11(1): 13059. doi: 10.1038/s41598-021-92438-y

[6] Didikoglu A, Mohammadian N, Johnson S, et al. Associations between light exposure and sleep timing and sleepiness while awake in a sample of UK adults in everyday life. Proceedings of the National Academy of Sciences. 2023; 120(42): e2301608120. doi: 10.1073/pnas.2301608120

[7] Benedetti M, Maierová L, Cajochen C, et al. Optimized office lighting advances melatonin phase and peripheral heat loss prior bedtime. Scientific reports. 2022; 12(1): 4267. doi: 10.1038/s41598-022-07522-8

[8] Schöllhorn I, Stefani O, Lucas RJ, et al. Melanopic irradiance defines the impact of evening display light on sleep latency, melatonin and alertness. Communications Biology. 2023; 6(1): 228. doi: 10.1038/s42003-023-04598-4

[9] Zandi B, Stefani O, Herzog A, et al. Optimising metameric spectra for integrative lighting to modulate the circadian system without affecting visual appearance. Scientific reports. 2021; 11(1): 23188. doi: 10.1038/s41598-021-02136-y

[10] Zandi, B., Eissfeldt, A., Herzog, A., & Khanh, T. Q. (2021). Melanopic Limits of Metamer Spectral Optimisation in Multi-Channel Smart Lighting Systems. Energies, 14(3), 527. DOI: 10.3390/en14030527

[11] Abeysekera, S. K., Kalavally, V., Ooi, M., & Kuang, Y. C. (2020). Impact of circadian tuning on the illuminance and color uniformity of a multichannel luminaire with spatially optimized LED placement. Optics Express, 28(1), 130-145. DOI: 10.1364/OE.381115

[12] Marín-Doñágueda M, Salgado-Remacha FJ, Jarabo S, et al. Simultaneous optimization of circadian and color performance for smart lighting systems design. Energy and Buildings. 2021; 252: 111456. doi: 10.1016/j.enbuild.2021.111456

[13] Wang Q, Dong J. Reinforcement learning control of multi-spectral LED systems for rendering optimal lighting performance in indoor environment. Building and Environment. 2024; 262: 111811. doi: 10.1016/j.buildenv.2024.111811

[14] Zeng Y, Sun H, Lin B. Optimized lighting energy consumption for non-visual effects: A case study in office spaces based on field test and simulation. Building and Environment. 2021; 205: 108238. doi: 10.1016/j.buildenv.2021.108238

[15] Trinh VQ, Bodrogi P, Khanh TQ. Determination and measurement of melanopic equivalent daylight (D65) Illuminance (mEDI) in the context of smart and integrative lighting. Sensors. 2023; 23(11): 5000. doi: 10.3390/s23115000

[16] Wang T, Li J, Wang Y, et al. Active interventions of dynamic lighting on human circadian rhythm and sleep quality in confined spaces. Building and Environment. 2022; 226: 109766. doi: 10.1016/j.buildenv.2022.109766

[17] Wang T, Shao R, Wang Y, et al. Impacts of Static Lighting in Confined Spaces on the Circadian Parameters, Alertness, Performance and Well-Being. Buildings. 2024; 14(4): 1115. doi: 10.3390/buildings14041115